Article:
Pulingam, T, Thong, KL, Ali, ME et al. (4 more authors) (2019) Graphene oxide exhibits differential mechanistic action towards Gram-positive and Gram-negative bacteria. Colloids and Surfaces B: Biointerfaces, 181. pp. 6-15. ISSN 0927-7765

https://doi.org/10.1016/j.colsurfb.2019.05.023

Graphical Abstract

Graphene Oxide Exhibits Differential Mechanistic Action towards Gram-positive and Gram-negative Bacteria

Thiruchelvi Pulingam [a], Kwai Lin Thong [b], Md. Eaqub Ali [a], Jimmy Nelson Appaturi [a]

Ignatius Julian Dinshaw [a], Zhan Yuin Ong [c], Bey Fen Leo [a,d*]

[a] *Nanotechnology & Catalysis Research Centre (NANOCAT), Institute of Graduate Studies, University of Malaya, 50603 Kuala Lumpur, Malaysia.*

[b] *Institute of Biological Sciences, Faculty of Science, University of Malaya, 50603 Kuala Lumpur, Malaysia.*

[c] *School of Physics and Astronomy and Leeds Institute of Biomedical and Clinical Sciences, School of Medicine, University of Leeds, Leeds LS2 9JT, U.K.*

[d] *Faculty of Medicine, University of Malaya, 50603 Kuala Lumpur, Malaysia.*

Graphical Abstract

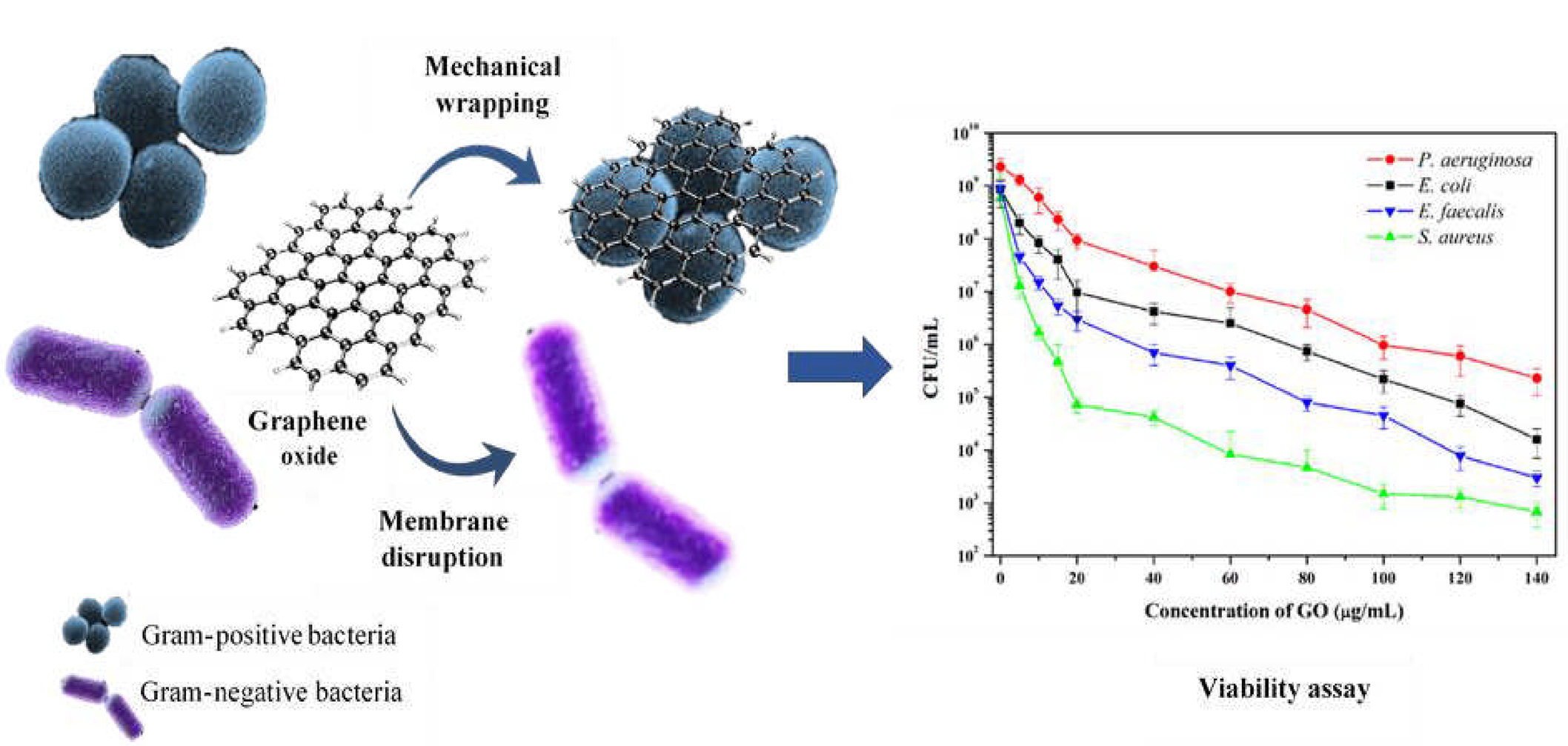

Highlights

- Antibacterial activity of GO towards bacteria are concentration and time-dependent.
- GO shows differential bactericidal activity towards bacteria.
- Mechanical wrapping was noted for *Staphylococcus aureus* and *Enterococcus faecalis.*
- Membrane disruptions was observed for *Escherichia coli* and *Pseudomonas aeruginosa*.

Graphene Oxide Exhibits Differential Mechanistic Action towards Gram-positive and Gram-negative Bacteria

Thiruchelvi Pulingam [a], Kwai Lin Thong [b], Md. Eaqub Ali [a], Jimmy Nelson Appaturi [a]

Ignatius Julian Dinshaw [a], Zhan Yuin Ong [c], Bey Fen Leo [a,d*]

[a] *Nanotechnology & Catalysis Research Centre (NANOCAT), Institute for Advanced Studies, University of Malaya, 50603 Kuala Lumpur, Malaysia.*

[b] *Institute of Biological Sciences, Faculty of Science, University of Malaya, 50603 Kuala Lumpur, Malaysia.*

[c] *School of Physics and Astronomy and Leeds Institute of Biomedical and Clinical Sciences, School of Medicine, University of Leeds, Leeds LS2 9JT, U.K.*

[d] *Faculty of Medicine, University of Malaya, 50603 Kuala Lumpur, Malaysia.*

Abstract

The antibacterial nature of graphene oxide (GO) has stimulated wide interest in the medical field. Although the antibacterial activity of GO towards bacteria has been well studied, a deeper understanding of the mechanism of action of GO is still lacking. The objective of the study was to elucidate the difference in the interactions of GO towards Gram-positive and Gram-negative bacteria. The synthesized GO was characterized by Ultraviolet-visible spectroscopy (UV-VIS), Raman and Attenuated Total Reflectance-Fourier-transform infrared spectroscopy (ATR-FTIR). Viability, time-kill and Lactose Dehydrogenase (LDH) release assays were carried out along with FESEM, TEM and ATR-FTIR analysis of GO treated bacterial cells. Characterizations of synthesized GO confirmed the transition of graphene to GO and the antibacterial activity of GO was concentration and time-dependent. Loss of membrane integrity in bacteria was enhanced with increasing GO concentrations and this corresponded to the elevated release of LDH in the reaction medium. Surface morphology of GO treated bacterial culture showed apparent differences in the mechanism of action of GO towards Gram-positive and Gram-negative bacteria where cell entrapment was mainly observed for Gram-positive *Staphylococcus aureus* and *Enterococcus faecalis* whereas membrane disruption due to physical contact was noted for Gram-negative *Escherichia coli* and *Pseudomonas aeruginosa*. ATR-FTIR characterizations of the GO treated bacterial cells showed changes in the fatty acids, amide I and amide II of proteins, peptides and amino acid regions compared to untreated bacterial cells. Therefore, the data generated further enhance our understanding of the antibacterial activity of GO towards bacteria.

Keywords: antibacterial activity, graphene oxide, mechanism of action, mechanical wrapping, membrane damage

* Corresponding author.

E-mail address: beyfenleo@um.edu.my (B.F. Leo).

1. Introduction

Graphene oxide (GO) is one of the promising materials that has been reported to have excellent antibacterial properties due to its easy and low cost of preparation and ability to be produced in a large-scale [1-3]. GO is the preferred nanomaterial in the biomedical field over other carbon allotropes because of its stability in colloidal form and the reliability of graphene's aqueous dispersibility when it is in a single or multi-layered state [4]. Ever since the first medical application of GO was demonstrated in the field of drug delivery in 2008, the research initiative in exploring other uses of graphene material in the biomedical field has been increasing exponentially [5-7].

The prevalence of multidrug-resistant pathogens has reduced the availability of effective drugs for the treatment of serious bacterial infections. Hence there has been intense interest to look for antimicrobial agents with alternative mechanisms of action. Metal/metal oxide nanomaterial such as silver, gold, titanium dioxide and zinc oxide have been used in the past decade as antibacterial materials to curb antibacterial resistance [8]. Although the antibacterial action of metal/metal oxide nanomaterials seems relevant in the past, these nanomaterials are not chemically inert [9]. This inadequacy may affect the stability and the antibacterial actions of metal/metal oxide nanomaterial, thus it is not recommended for long-term use especially in the clinical application [10].

One of the current applications is the use of GO as an antibacterial material. The antibacterial property of GO is attributed to the direct physical and chemical activity of GO on the bacterial membrane [11]. Loss of microbial membrane integrity and the leakage of intracellular content have been reported to be one of the key mechanisms of bacterial inhibition by GO [12]. Therefore, GO may have the potential to be an effective antibacterial material to reduce the excessive use of antimicrobials [13]. Additionally, the difference in the

cell wall components of the Gram-positive and Gram-negative bacteria also contributes to the better antibacterial activity of GO towards *S. aureus* than *E. coli* [14, 15]. Although the antibacterial activity of GO is increasingly reported, the detailed mechanism of action is still lacking and poorly understood [16].

In this study, GO was prepared and their antibacterial activity was evaluated against Gram-positive (*Staphylococcus aureus*, *Enterococcus faecalis*) and Gram-negative (*Escherichia coli, Pseudomonas aeruginosa*) bacteria. Specifically, cell viability and kinetic studies were carried out while field emission scanning electron microscopy (FESEM) techniques were conducted to observe the difference in the bacterial surface morphology before and after exposure to GO. Transmission electron microscopy (TEM) analysis was carried out for the treated bacterial cells to determine the effects of GO on cell morphology. Finally, ATR-FTIR characterizations of untreated and GO-treated bacteria were conducted to examine their interaction mechanisms.

Although there were many studies on the antibacterial activity of GO against Gram-positive and Gram-negative bacteria, however the difference in the mechanism was not dealt with [14, 17-20]. Here, we report the difference in the activity of GO towards Gram-positive and Gram-negative bacteria based on FESEM, TEM and LDH analyses. To the best of our knowledge, this is the first report that provides evidence for the dissimilarity in the mechanistic actions of GO. Additionally, we have described the mechanism of action GO towards bacteria at molecular level through ATR-FTIR characterizations of untreated and GO-treated bacteria.

2. Materials and Methods

2.1. Materials

Graphite powder, H_2SO_4, H_2PO_4, HCl, H_2O_2 and $KMnO_4$ were purchased from Sigma-Aldrich, USA. Phosphate buffered saline (PBS) was prepared using PBS tablets from Sigma-Aldrich, USA. Tryptic Soy Agar (TSA) and broth (TSB) were prepared using dehydrated bacterial culture media from BD Difco™, USA. Bacterial cultures *S. aureus* ATCC 25923, *E. faecalis* ATCC 29212, *E. coli* ATCC 25922 and *P. aeruginosa* ATCC 27853 were from the culture collection of Biomedical Science Laboratory, University of Malaya, Kuala Lumpur, Malaysia.

2.2. Synthesis and characterization of GO

GO sheets were prepared through the modified Hummer's method [21, 22]. Ultraviolet absorption spectra were obtained using Lambda 35 (Perkin-Elmer, USA). An aqueous solution of GO was used as the sample for UV-Vis and distilled water was used as the reference. Wavelengths from 200 to 700 nm were used to characterize the GO. Raman spectra of GO sheets were obtained using a Renishaw inVia Raman microscope (UK) with an excitation laser wavelength of 325 nm. The excitation was conducted with a He-Ne laser in the regions of 1000 to 2200 cm^{-1}. ATR-FTIR characterization of GO was done using Spectrum 400 IR spectrometer equipped with diamond crystal (Perkin Elmer, USA). The ATR-FTIR spectra were recorded with a resolution of ± 4 cm^{-1} and a scan number of 12 in the range of 4000 to 400 cm^{-1}.

2.3. Bacterial culture conditions

The bacterial stock cultures were revived and streaked on Tryptic Soy Agar (TSA) plates to check for purity. The culture plates were incubated overnight at 37 °C. A single colony from

the overnight TSA was picked and used to inoculate 10 mL Tryptic Soy Broth (TSB). The inoculated broth was incubated overnight at 37 °C with agitation (150 rpm).

2.4. Bacterial Viability Assay

An aliquot of 5 mL of bacterial cultures (10^8 cfu) was incubated with GO of varying concentrations ranging from 5 to 140 μg mL^{-1} for 4 h at 37 °C with agitation (150 rpm). At the end of the designated time period, an aliquot of 100 μL was withdrawn and serially diluted (1:10) in 0.8% saline solution. Serially diluted cell suspensions were plated onto the TSA and incubated overnight at 37 °C to determine the bacterial counts (cfu). The assay was carried out in triplicates of three independent experiments and the results were averaged. The degree of bacterial inactivation was calculated using the formula: $(T_0 - T)/ T_0$ where T_0 is the number of bacteria in the GO-free reaction and T is the residual bacteria in the reaction medium at a certain GO concentration. Three independent replicates were conducted for the assay.

2.5. LDH Cytotoxicity Assay

The release of LDH cytotoxicity assay was conducted to determine the degree of membrane damage of bacteria once treated with GO. Membrane integrity of treated bacteria was evaluated using LDH Cytotoxicity Assay Kit (Thermo Fisher Scientific, Massachusetts, USA). Bacterial cultures (10^8 cfu) were incubated with GO suspension of varying concentration ranging from 5 – 140 μg mL^{-1} for 4 h at 37 ºC with agitation (150 rpm). At the end of the time period, 50 μL of each reaction mixture were transferred to a 96-well plate and the assay was carried out according to the manufacturer's instructions. The absorbance was measured using a microplate spectrophotometer (Epoch-BioTek, Vermont, USA). Untreated bacterial cultures were regarded as negative control and three independent experiments were performed with replicates and the results were averaged.

2.6. *Time-kill assay*

Standardized bacterial cultures (10^8 cfu) were incubated with 10 µg mL^{-1} of GO suspension at 37 °C with gentle agitation (100 rpm). At the end of selected time periods (2 h, 4 h, 6 h and 8 h), 100 µL of the bacterial culture was withdrawn and serially diluted (1:10) in 0.8% saline solution. Serially diluted cell suspensions were then plated onto the TSA and incubated overnight at 37 °C. Three independent experiments were carried out in triplicates and the results were averaged.

2.7. *Observation of bacterial cell morphology upon GO treatment*

GO treated and untreated bacterial cells were retrieved from respective experiments for further surface morphology observations. Briefly, 1 µL of the bacterial suspension (~ 10^8 cfu mL^{-1}) were treated with 4 % glutaraldehyde (GLA) for 30 minutes, washed with cacodylate buffer and further fixed with 1% Osmium tetroxide for another 30 minutes. The fixed bacterial cells were then gradually dehydrated with ethanol using increasing concentrations ranging from 30%, 50%, 70%, 80%, 90%, and finally 100%. Each ethanol wash was performed for 15 minutes and finally, the completely dried bacterial cells were sputter coated with gold for FESEM observations (FEI, Quanta FEG 650) at a working distance around 9 mm, with an acceleration voltage of 20kV. The GO treated bacterial isolates were also observed under TEM (Carl Zeiss, LEO LIBRA 120). For the TEM sample preparation, treated bacterial cells were fixed with 4 % GLA for more than 4 h and washed with cacodylate buffer, fixed with 1% Osmium tetroxide for 2 h and washed again with cacodylate buffer. The bacterial cells were then dehydrated through a graded series of ethanol, treated

using propylene oxide and finally embedded in Epon. Thin sections were cut through ultramicrotome, stained with uranyl acetate, air-dried and viewed under TEM.

2.8. ATR-FTIR characterizations of GO and bacteria interactions

Bacterial cultures were treated with 10 μg mL^{-1} of GO for 4 h as described in the previous section. An aliquot of 100 μL of the GO-treated and untreated bacterial (control) cultures was aseptically dropped onto glass slides, respectively and left to dry. The thin film was analyzed through Spectrum 400 IR spectrometer equipped with diamond crystal (Perkin Elmer, USA). Spectra were recorded with a resolution of ± 4 cm^{-1} and scan number of 12 in the range of 4000 to 400 cm^{-1}.

3. Results and Discussion

3.1. Characterizations of GO

The modified Hummer's method has enabled the formation of an oxidized graphite material that could be further sonicated to form an aqueous suspension of GO. The prepared GO sheets were characterized using ultraviolet adsorption spectroscopy. As seen from Fig.1(a), a peak which corresponds to the π - π* plasmon was observed at around 240 nm due to sp^2 clusters of the GO and linking units such as C=C, C=O, and C-O bonds. The shoulder band from 290 nm to 300 nm can be attributed to the n – π* transitions of C = O bonds [23, 24], consistent with the findings reported by Gupta *et al.* [25] and Luo *et al.* [26]. Raman spectroscopy is a powerful nondestructive technique and is a very useful optical approach to distinguish the ordered and disordered structure of carbonaceous materials [27, 28]. The Raman spectrum of graphene oxide is shown in Fig. 1(b). Two clear bands at 1416 cm^{-1} and 1598 cm^{-1} are the dominant vibrational modes corresponding to the D and G bands of carbon,

respectively [18]. The intense G band at 1598 cm^{-1} is common to all sp^2 carbon forms and is attributed to the optically allowed E_{2g} phonon. The weak D band at 1416 cm^{-1} is ascribed to the mode of the κ-point phonons of A_{1g} symmetry [29], reflecting the degree of defects found on the structure. Raman spectroscopy is mostly used to acquire structural data on carbon materials [30]. The strong band (G) is due to the sp2-bonded carbon regions while the weaker band (D) reflects the degree of defects found on the structure [31].

The ATR-FTIR spectrum of GO is shown in Fig. 1(c). The presence of the bands in this spectrum is associated with the functional groups of GO. Vibration modes that are based on the configuration of oxygen which include the OH, C-OH, COOH and C-O functional groups are observed in the GO spectrum. The peak observed at 3224 cm^{-1} could be attributed to the presence of carboxyl O-H stretching vibration mode. This peak appeared broad as it overlaps with absorption peaks that correspond to O-H stretching due to the presence of absorbed water molecules and alcohol groups [32]. The asymmetric CH_2 stretching of GO appears at 2930 cm^{-1} and the band that appears as a shoulder peak at 1735 cm^{-1} is attributed to C=O stretch of carboxyl group [33]. The bands at 1397 cm^{-1} and 1053 cm^{-1} corresponds to C-OH and C-O stretching vibrations, respectively [34].

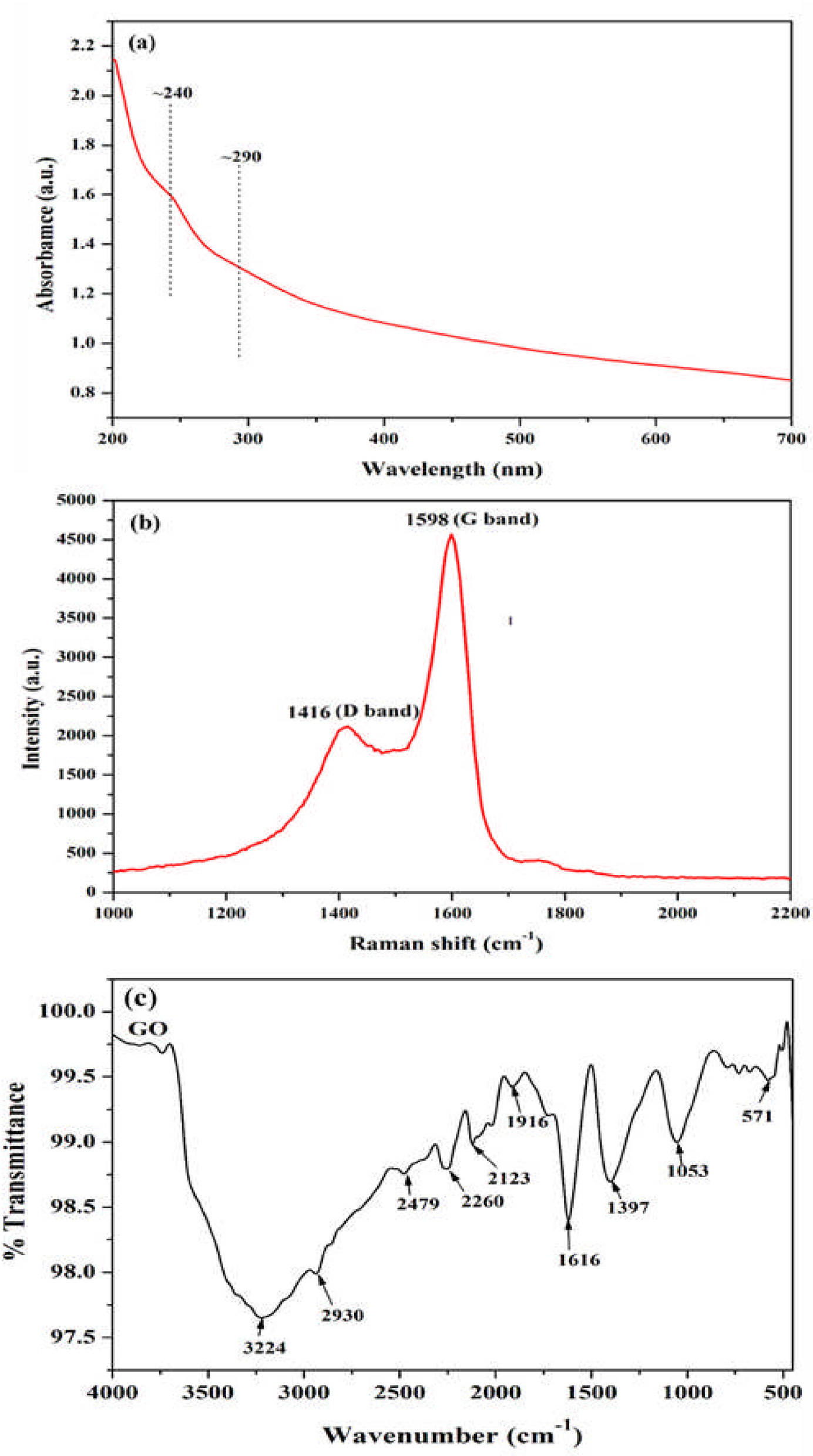

Fig. 1. Characterization of synthesized GO using UV-Vis and Raman spectroscopy. (a) UV-Vis spectrum of GO; absorbance peak of π - π^* plasmon is observed at 240 nm. (b) Raman spectrum of GO; G band arises due to the sp2-bonded carbon regions and the D band reflects the degree of defects found on GO. (c) ATR-FTIR spectrum of GO; Functional groups of OH, COOH, C-OH and C-O are indicated at 3224 cm^{-1}, 1735 cm^{-1}, 1397 cm^{-1} and 1053 cm^{-1}, respectively.

3.2. *Concentration-dependent activity of GO*

The antibacterial activity of GO was assessed by exposing selected Gram-positive and Gram-negative bacteria to various concentrations of an aqueous suspension of GO ranging from 0 to 140 μg mL^{-1} for a fixed time-period (4 hours). The line graph in Fig. 2(a) clearly depicts the reduction in the number of cells with an increasing GO concentration for all bacterial strains. The cfu counts indicated that GO has almost completely inhibited the bacterial growth of all strains as seen in the line graph, but the inactivation rate differed among individual bacteria at lower concentrations. Increasing concentrations of GO nearly inactivated 99.9% of all bacteria, whereas *S. aureus* was almost fully inactivated at GO concentrations of 5 μg mL^{-1} compared to other strains. More than 99.9% reduction (> 3 log reductions) in colony counts signifies the bactericidal effect of the GO sheets. Similar observations were made by Akhavan *et al* [14] who reported that *S. aureus* cells have higher susceptibility to GO nanowalls compared to *E. coli*. They reported that the RNA efflux was higher for *S. aureus* than for *E. coli* when exposed to the same concentrations of GO [14].

Additionally, membrane integrity of GO treated bacterial cultures was measured by monitoring the release of LDH into the reaction medium after treatment. LDH cytotoxicity assay is commonly used to evaluate the loss of membrane integrity of cells after treatment with toxic compounds [35]. It was found that exposure of bacteria to increasing concentrations of GO enhanced the levels of LDH detected in the medium. This was noted for all bacteria for increasing GO concentrations however differences in the levels of detectable LDH among the bacterial cultures were noted as shown in Fig. 2(b). Higher release of LDH was observed for the Gram-positive isolates (*S. aureus and E. faecalis*) compared to the Gram-negative isolates (*E. coli and P. aeruginosa*). At 10 μg mL^{-1} of GO, 92% and 83.3% of cytotoxicity level were noted for *S. aureus* and *E. faecalis* respectively while

cytotoxicity levels of 66.7% and 58.3% were noted for *E. coli* and *P. aeruginosa* respectively.

In this study, we have tested two Gram-positive bacteria *S. aureus* and *E. faecalis* and two Gram-negatives *E. coli* and *P. aeruginosa*. Our study indicated that the degree of bacterial inactivation followed the order; *S. aureus* > *E. faecalis* > *E. coli* > *P. aeruginosa* in a descending trend. Evidently, membrane structure plays a definite role in determining the antibacterial activity of GO [14]. Increasing GO concentrations resulted in a reduction in the viability of all strains and enhanced release of LDH, most notably for *S. aureus* and the least towards *P. aeruginosa*, therefore the bactericidal activity of GO is concentration-dependent. This observation concurred with other reports [23, 36, 37]. The higher concentrations of GO provided increased contact with bacterial cells in which the abundant GO sheets could entrap bacterial cells through the wrapping mechanism.

The wrapping mechanism explains that GO separates the bacterial cells from the nutrients that are present in the growth medium, thus inhibiting cell proliferation resulting in cell death [31, 38]. As GO concentrations of 10 μg mL^{-1} was able to inactivate more than 60% of live cells, this concentration was selected for subsequent experiments. A similar study also reported that 10 μg mL^{-1} of GO suspension was able to exert toxic effects towards bacteria as higher concentrations would possibly cause indirect toxic effects through cell entrapment mechanism which separates bacterial cells from the reaction medium [10].

261

262

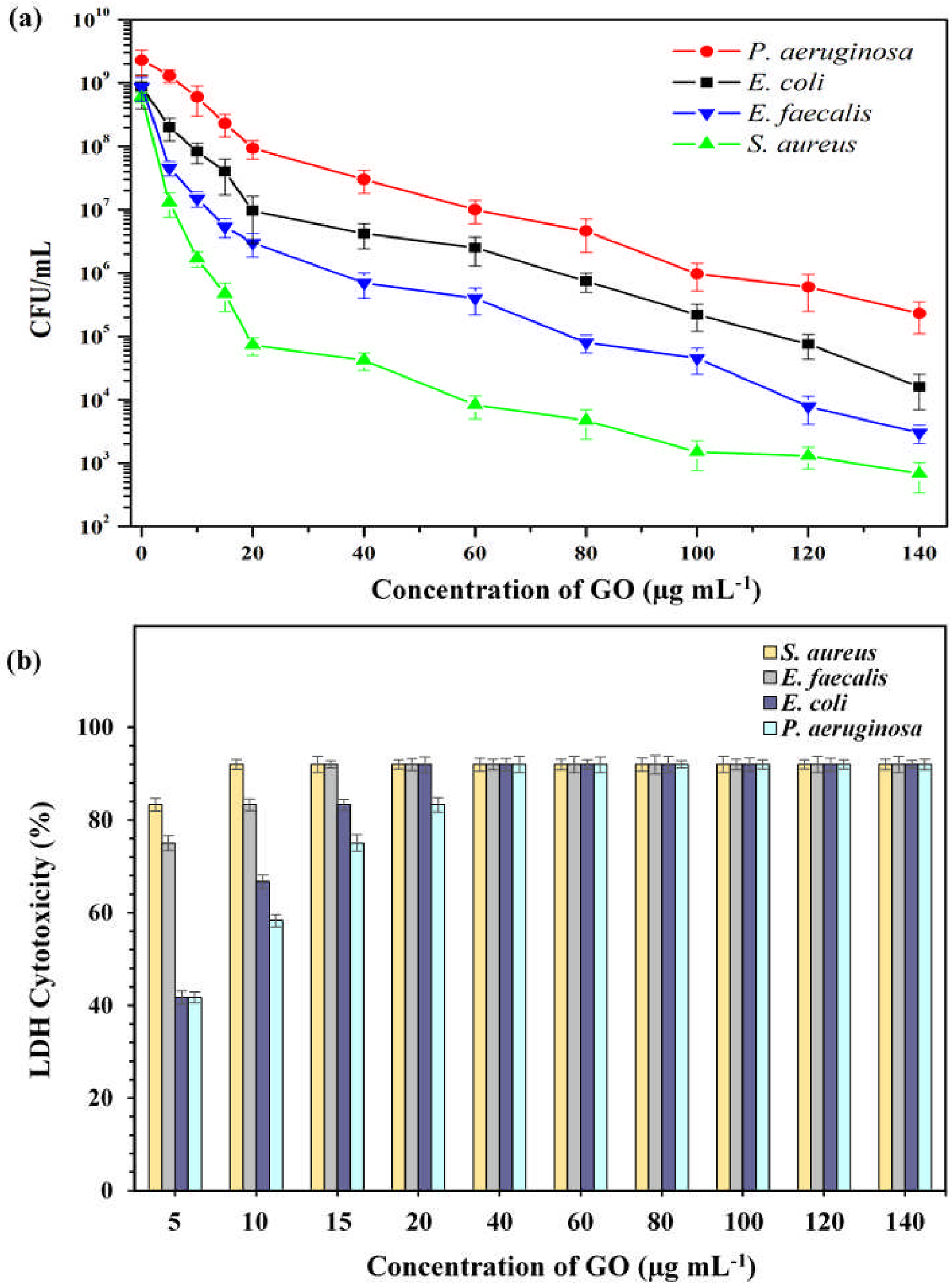
(a)
CFU/mL
Concentration of GO (μg mL-1)
P. aeruginosa
E. coli
E. faecalis
S. aureus
(b)
LDH Cytotoxicity (%)
Concentration of GO (μg mL-1)
S. aureus
E. faecalis
E. coli
P. aeruginosa

263

Fig. 2. Viability curve and LDH cytotoxicity analyses of bacteria after exposure to GO for 4 h. (a) A sharp decrease in the viability was observed at GO concentration of 10 μg mL^{-1} and deteriorates further as the concentration of GO increases. (b) Increased levels of LDH was measured for increasing concentrations of GO.

3.3. Time-dependent activity of GO

Time-dependent assays were performed for 8 h with a 2-hour interval time at a fixed GO concentration (10 μg mL^{-1}) for all the tested strains. Loss of viability increased with a longer period of incubation as all strains recorded the highest amount of cell death at the 8th hour (Fig. 3). This time-dependent assay also followed the same order of inactivation; *S. aureus* > *E. faecalis* > *E. coli* > *P. aeruginosa*. A large portion of cell death occurred at 4 h of incubation and this time-period was used in the subsequent investigations in this work to explore the interactions of GO. Furthermore, Gurunathan *et al.* [23] and Liu *et al*. [37] also described that a major proportion of cell death occurred in the early hours of incubation time which is consistent with our study. This phenomenon suggests that increasing incubation time contributes to longer interaction time and improved contact of GO sheets towards bacterial cells. Although more than 60% viability loss were seen at the 4th hour, better contact mediates enhanced antibacterial activity and this has resulted in major cell loss especially at the 8th hour of incubation. Additionally, with increasing time of contact, the overall proliferation of bacteria may be hindered because a large proportion of bacteria were rendered non-viable at early hours of incubation time. Therefore, our results indicated that the antibacterial activity of GO is concentration- and time-dependent.

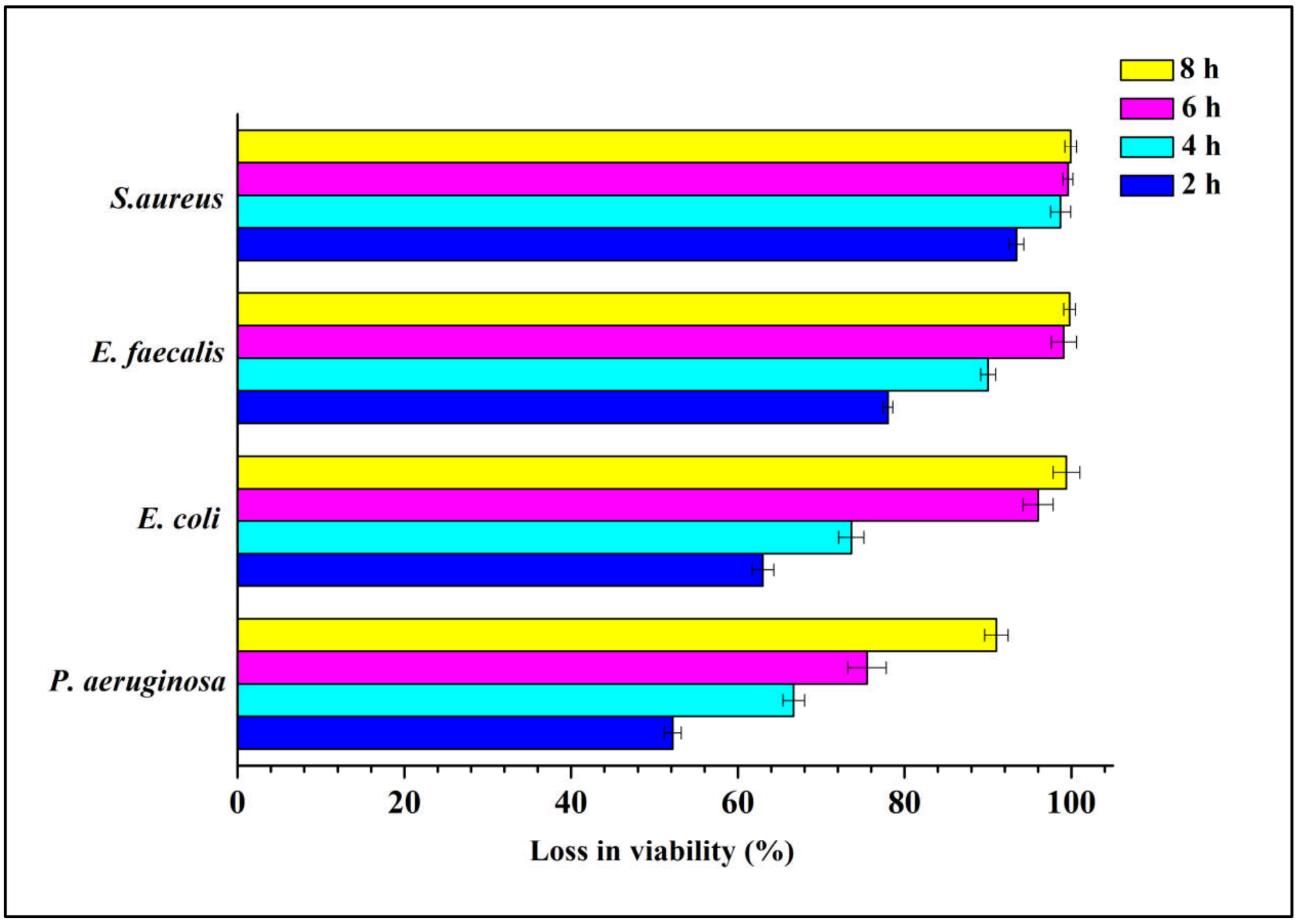

Fig. 3. Time kill assay of bacteria after exposure to GO for several time periods (2 h, 4 h, 6 h and 8 h). Increase in the incubation time improves bacterial cell contact with GO and this leads to higher percentage of cell death.

3.4. Visualization of the bacterial cell upon exposure to GO

FESEM characterizations were conducted to investigate the interactions between the bacterial cell membrane and GO sheets. Fig. 4A – 4D represent untreated bacterial cells while Fig. 4E - 4H show the treated cells. FESEM images revealed that untreated bacterial cells were observed to have intact cell membrane compared to bacterial cells that were treated with GO. Treated bacteria cells showed deformed shapes for all strains which indicated compromised membrane integrity and resulted in eventual cell death.

Besides, TEM analyses were carried out to monitor morphological changes in the bacterial cells after treatment with GO. Fig. 5A – 5D show the TEM images of untreated bacteria while Fig. 5E – 5H indicate the mechanism of interaction of GO towards bacterial cells. The degree of membrane disruptions and mechanism of action vary according to the type of bacteria. A clear difference in the degree of membrane damage and methods of GO interactions could be observed in the FESEM and TEM images between Gram-positive and Gram-negative bacteria. Large clusters of Gram-positive *S. aureus* and *E. faecalis* appeared to be entrapped by numerous GO sheets in both the FESEM and TEM images. The wrapping mechanism of bacterial cells *via* GO sheets is a documented antibacterial mechanism of action where the cells are actively isolated from the nutrient medium and undergo cell death [31]. In our study, this mechanism was observed clearly for the Gram-positive cells only. As Gram-positive bacteria (*S. aureus* and *E. faecalis*) are usually present in clusters, this increased the surface area of exposure to GO sheets and these cells get trapped leading to the higher death rate. The total surface area of the Gram-positive cells exposed to GO sheets is higher as these bacterial cells (*S. aureus* and *E. faecalis*) usually occur in clusters. Hence more cells are trapped, leading to higher cell death.

In contrast, the Gram-negative bacteria suffered hollows and dents on their membrane surface and did not appear to be severely trapped under GO sheets, unlike the Gram-positive cells as observed in Fig. 4G and 4H. Although membrane corrugations have been mainly observed for the Gram-negative bacteria only, loss of viability among *E. coli* and *P. aeruginosa* were lower compared to Gram-positive bacteria. In addition, the TEM images of the Gram-negative bacteria in Fig. 5G and 5H were observed to display a decrease in intracellular density which indicated minor loss of cellular components. This type of membrane damage is the effect of physical disruption where destructive extraction of lipid molecules may have occurred. A similar observation was reported by Tu *et al.* [39] that GO treated bacterial cells suffered lower surface phospholipid density due to partial membrane damage. For instance, *E. coli* has been observed to display a slight loss in cytoplasmic content where gaps existed between the cytoplasm and cell wall in the TEM images (Fig. 5G). Similar observations were made by Hu *et al*. [40] and Li *et al*. [41] where bacterial cells treated with GO appear to have suffered a loss in cellular integrity along with leakage of cytoplasmic content. Liu *et al.* [37] indicated that the membrane damage happens only after a direct contact with graphene-based materials and the damage appears to be irreversible. The difference in the loss of viability between Gram-positive and Gram-negative bacteria may be explained by the tendency of the Gram-positive bacteria to form cell clusters besides the apparent difference in the cell wall structure. In contrast, Gram-negative bacteria are usually present in single or paired cells, thus a lesser number of bacterial cells will be exposed to GO at any given time, hence lower viability loss for the Gram-negative bacteria was found in this study [42]. Therefore, the antibacterial potential of GO is influenced by the degree of contact between bacterial cells and GO sheets. Similarly, a study conducted by Perreault *et. al.* [31] also reported that the close contact between the GO sheets and bacteria cells could compromise the integrity of bacterial membranes.

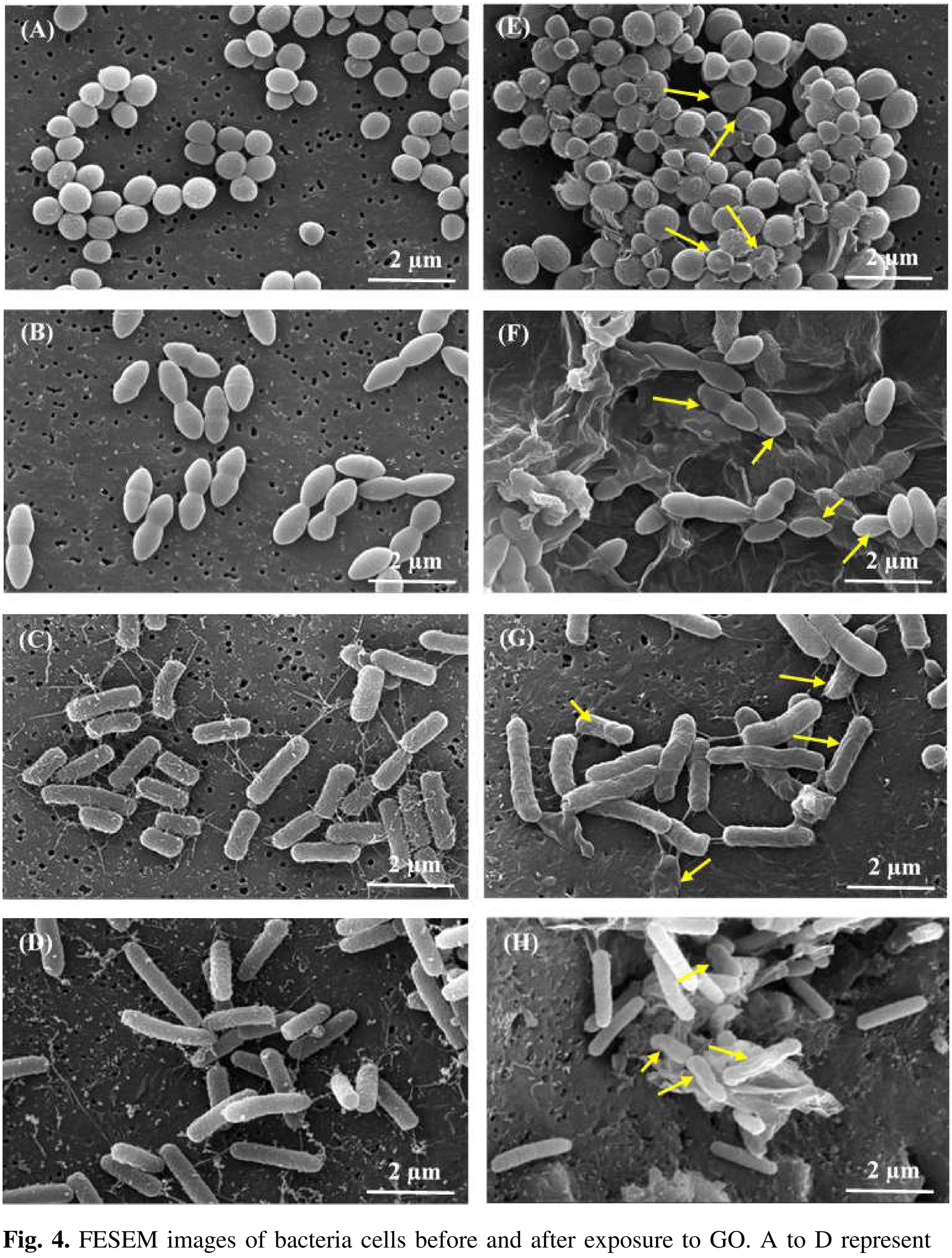

Fig. 4. FESEM images of bacteria cells before and after exposure to GO. A to D represent untreated bacteria and E to H represent GO-treated bacterial cells. (A and E; *S. aureus*, B and F; *E. faecalis*; C and G; *E. coli*, D and H; *P. aeruginosa*.) Yellow arrows indicate membrane damage that was observed under FESEM analysis for GO-treated cells only.

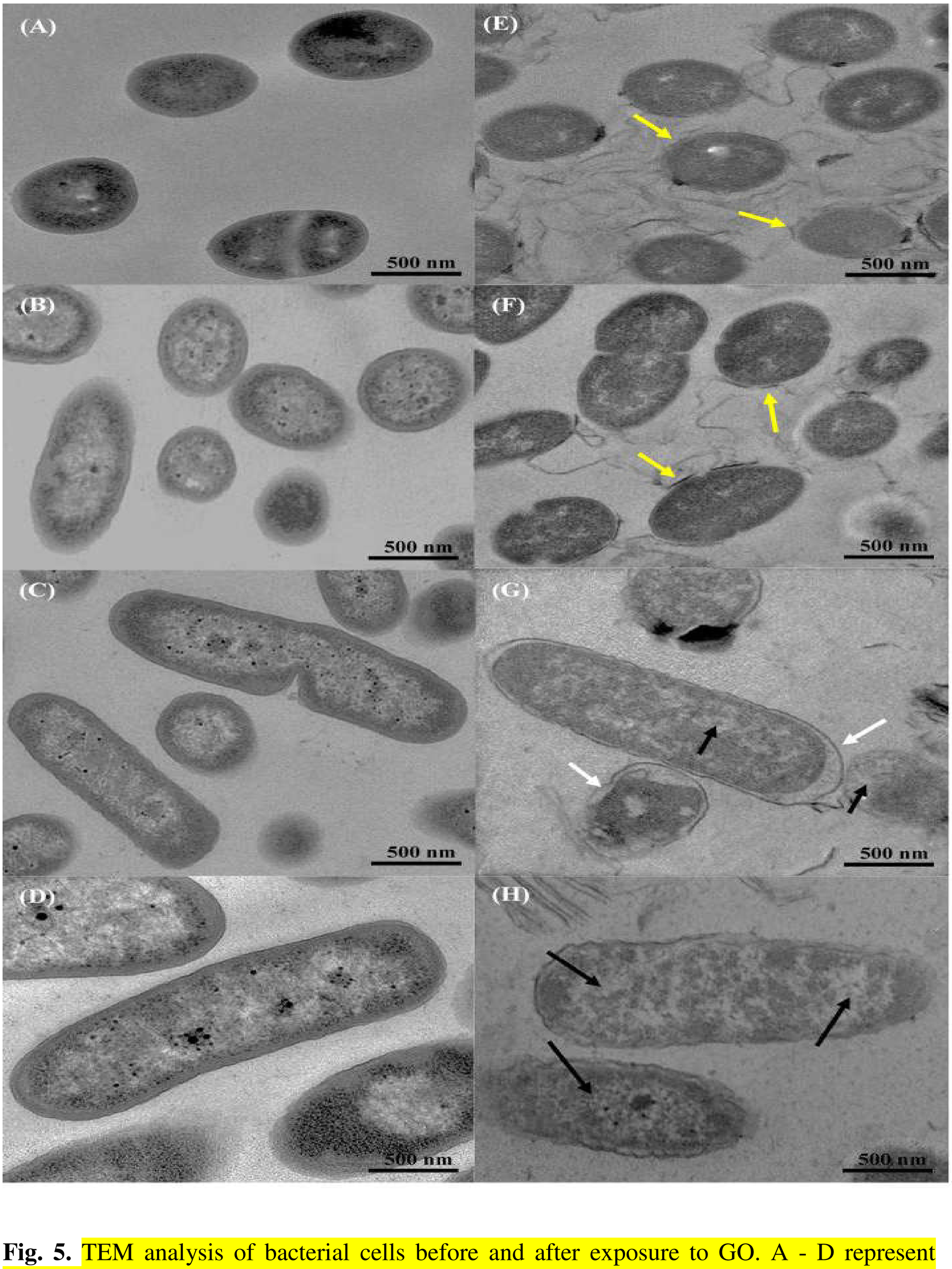

Fig. 5. TEM analysis of bacterial cells before and after exposure to GO. A - D represent untreated bacteria and E to H represent GO-treated bacteria. (A and E; *S. aureus*, B and F; *E. faecalis*; C and G; *E. coli*, D and H; *P. aeruginosa*). Yellow arrows indicate attachment of GO sheets onto bacterial cells to potentiate antibacterial mechanism. White arrows show detachment of cell membrane that may have been caused by leakage of cell content. Black arrows indicate lower density of lipids that may have been caused by partial membrane damage.

3.5. ATR-FTIR characterizations of GO and bacteria interactions

ATR-FTIR spectra of bacterial cells are usually conducted to analyze the surface chemistry and functional groups that are present on the cell walls of the bacteria [43]. This technique is commonly used for the identification, detection and classification of bacteria [44, 45]. It is also used to detect changes at the molecular level in bacterial cell wall structure. The ATR-FTIR spectra of untreated and GO-treated bacterial cells were analyzed to deduce the different actions of GO on Gram-positive and Gram-negative bacteria.

Amongst the bands that exhibited clear differences, the 2344 cm^{-1} band in GO-*S. aureus* was assigned to the O-H stretching due to the carboxylic acid which is also present in the GO framework [46]. However, the intensity of the peak was reduced and the peak was observed to be shown at 2260 cm^{-1} in the bare GO spectrum (Fig. 6). The primary and secondary amides (region II) of *S. aureus* occurred at 1622 cm^{-1} and 1538 cm^{-1}, respectively due to the stretching vibrations of C=O and N-H [47]. The intensity of both C=O and N-H bands decreased after the introduction of GO. Additionally, the presence of amino acid functional group at 517 cm^{-1} (region V) which is due to the COO^- and the symmetric C=O stretching of amino acids at 1392 cm^{-1} (region III) were diminished in the GO-*S. aureus* spectrum as shown in Fig. 6(a) [48]. The exposure of GO in the *S. aureus* culture has introduced changes in the carboxylic group of fatty acids, primary and secondary amides of proteins, peptides and amino acids. This might have played a role in causing more damage to the cell wall of these bacteria. The ATR-FTIR spectra of *E. faecalis* and GO-*E. faecalis* are shown in Fig. 6(b). The presence of the characteristic bands of C-H asymmetric of CH_2 in fatty acids at 2939 cm^{-1} in GO-*E. faecalis* spectrum has almost disappeared [46]. Furthermore, the O-H stretching vibration due to carboxylic acid at 2319 cm^{-1} and C≡C stretching vibration of monoalkyl acetylene at 2132 cm^{-1} have also been reduced in GO-*E.*

faecalis spectrum [34]. The decrease in the intensity of the peaks from region II to region V reflects the chemical transformation taking place after the treatment of *E. faecalis* with GO.

Fig. 6(c) shows the ATR-FTIR spectra of *E. coli* and *E. coli* treated with GO. The peak at 2923 cm^{-1} in *E. coli* spectrum is due to the presence of C-H stretching in aliphatic compounds of cell walls such as lipids mainly along with a minor contribution from proteins, carbohydrates and nucleic acids [34]. This peak, however, has intensified in the GO - *E. coli* and GO -*P. aeruginosa* spectra as well. The intensity of amide II (protein N-H bend, C-N stretch) peak at 1535 cm^{-1} in GO-*E. coli* spectrum has noticeably reduced [49]. Moreover, the peak attributed to COO- symmetric stretch in amino acid side chains and fatty acids at 1391 cm^{-1} slightly reduced and have shifted to 1378 cm^{-1}. Furthermore, a P=O asymmetric stretching band which appeared at 1228 cm^{-1} is mainly due to nucleic acids with some influence from phospholipids [50]. These peaks do not fluctuate before and after the treatment. The strong absorption band that appeared at 1059 cm^{-1} may be associated with PO^{2-} symmetric stretching from nucleic acids and phospholipids and this band decreases in intensity after GO treatment [51]. Similarly, the PO^{2-} symmetric stretching band appeared at 1070 cm^{-1} for *P. aeruginosa* and this band decreased in intensity after GO exposure. The ATR-FTIR spectra of *P. aeruginosa* and GO-P. *aeruginosa* is shown in Fig. 6(d). In contrast to other bacteria, the amide I and amide II bands of *P. aeruginosa* after the GO treatment have intensified. Therefore, the results clearly demonstrated the differential effects of GO on the functional groups on the surface of the bacterial cell walls.

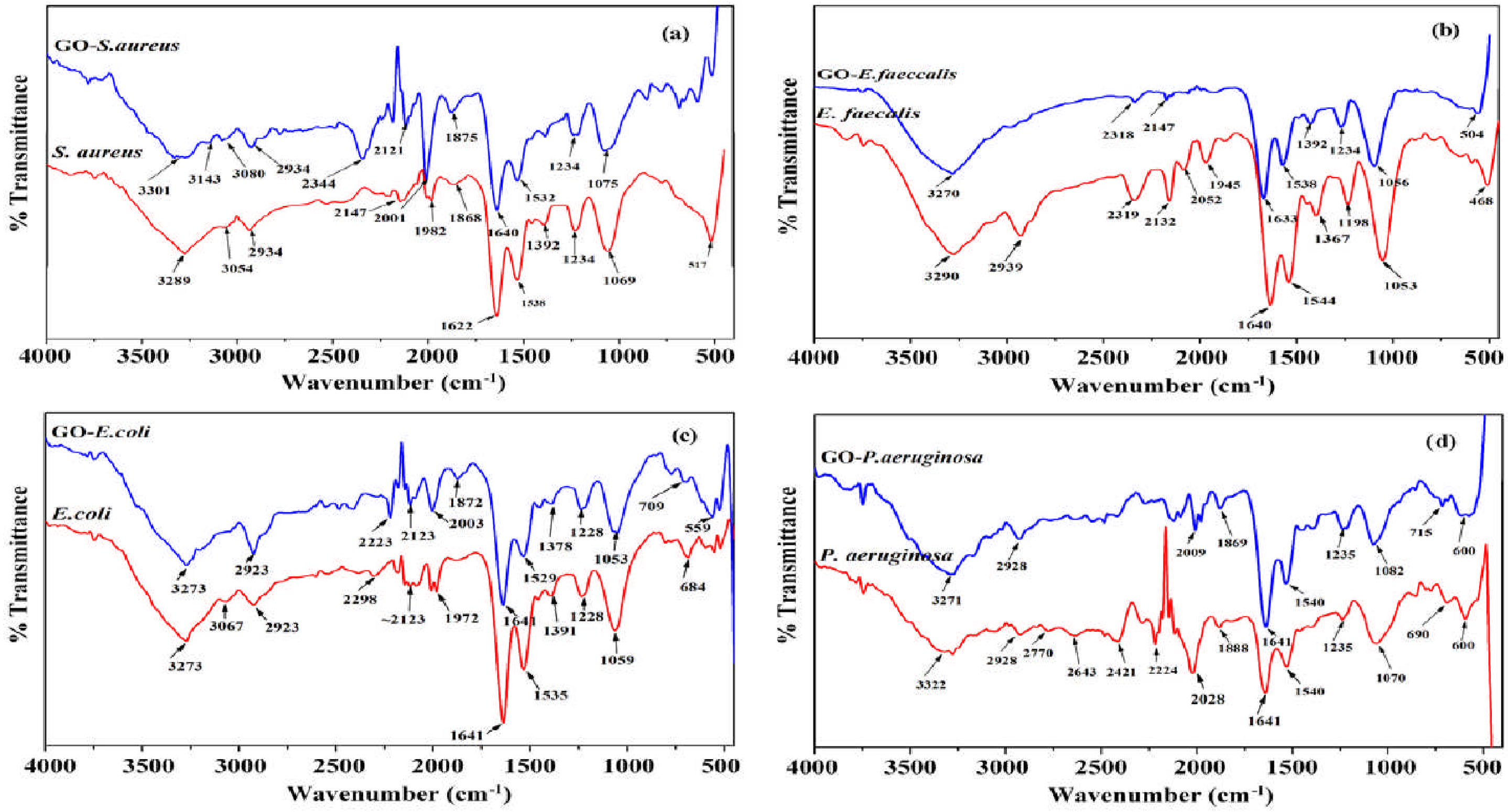

405 **Fig. 6.** ATR-FTIR characterizations of untreated and GO treated bacterial cultures. The spectra show the differences in the intensity of
406 functional groups that are present on the surface of bacterial cell wall before and after treatment with GO. (a) ATR-FTIR spectra of untreated
407 and treated *S. aureus*; (b) ATR-FTIR spectrum of untreated and treated *E. faecalis*; (c) ATR-FTIR spectrum of untreated and treated *E. coli*; (d)
408 ATR-FTIR spectrum of untreated and treated *P. aeruginosa*.

3.6. *Mechanism of action of GO towards bacteria*

Our study showed that the antibacterial effects of GO on Gram-positive bacteria were greater compared to Gram-negative bacteria. Additionally, ATR-FTIR characterizations of untreated and treated bacterial isolates confirmed molecular interactions that occurred between the bacterial cell and GO sheets. Briefly, the exposed part of the bacteria that is available for the GO to immediately act on is the outer membrane layer for Gram-negative bacteria and the peptidoglycan layer for Gram-positive bacteria [52]. This dissimilarity plays a role in determining the type of interactions that occur between the two classes of bacteria with GO. Similar observations were made by Deokar *et al*. [15] who reported that Gram-positive *S. aureus* was more susceptible towards the antibacterial activity of carbon nanotube compared to Gram-negative *E. coli*. The authors suggested that Gram-positive bacteria interacted with these nanomaterials through electrostatic or hydrogen bonding besides physical piercing of cell membrane while Gram-negative bacteria interacted with the nanomaterial through direct physical contact only [15].

The thick peptidoglycan layer in Gram-positive bacteria and additional presence of teichoic acids, lipoids and amino acids on the surface of these bacteria may have contributed to the added interaction between the Gram-positive bacteria and GO [15, 53]. The peptidoglycan layers have an adherence characteristic which may have caused this layer to behave as a chelating agent [54] and this can be attributed to the presence of surface proteins such as teichoic acids and adhesins [55]. In general, Gram-positive bacteria such as *S. aureus* and *E. faecalis* are commensal bacteria on humans where the former resides on the skin and the latter resides in the gastrointestinal tract [56, 57]. However, these bacteria are also opportunistic pathogens which could cause invasive infections when there is a breach in the epithelial lining by adhering to the host tissues to initiate bacterial colonization [55]. Therefore, we propose that similar adhering mechanism has prompted interactions with the

GO sheets, whereby the surface proteins on the peptidoglycan layer have interacted with GO. The interactions of GO with Gram-positive bacteria may have contributed to the mechanical wrapping of GO sheets onto *S. aureus* and *E. faecalis* as indicated in Fig. 7(A) and 7(B). Thus, the peptidoglycan layer tends to interact with GO sheets once it is in close proximity and this necessitates adherence of GO onto the bacterial membrane.

FESEM images in Fig. 4 show that GO sheets are observed to entrap *S. aureus* and *E. faecalis,* however, this is not the case for Gram-negative *E. coli* and *P. aeruginosa.* The outer membrane layer on Gram-negative bacteria forms an extra protective layer for these bacteria from interacting closely to GO sheets. Although membrane damage to *E. coli* and *P. aeruginosa* have been observed, mechanical wrapping of these cells was not observed in the FESEM or the TEM images. Therefore, variation in the degree of damage on the bacterial membrane among the Gram-positive and Gram-negative bacteria may be contributory to the type of interaction that occurred during contact between bacteria and GO sheets [15]. The outer membrane is essential to the survival of Gram-negative bacteria as this layer offers protection to the bacteria in a hostile environment including in the presence of antibiotics and it is one of the key reasons that Gram-negative bacteria are generally resistant towards antibiotics [58]. The lipopolysaccharide (LPS) that is found on the outer leaflet of the outer membrane plays a role in the effective exclusion of hydrophobic molecules [55, 59]. It was suggested LPS molecules may contribute to the overall repulsive forces on Gram-negative bacteria through steric repulsion [60].

It has been noted that interaction between the bacteria and GO are mainly repulsive as reported by Castrillón *et al.* [61] who investigated the effects of GO - functionalized atomic force microscopy (AFM) probe puncture on *E. coli* cell wall. The repulsive force may have arisen from the electrostatic repulsion from the negatively charged bacterial outer membrane and deprotonated carboxylic acid groups existing on GO [62, 63]. However, sporadic

adhesions were measured upon AFM probe pull-off and it was suggested to be due to LPS stretching effects which bridges cell surface and AFM tip upon pull-off [61]. In our study, similar events may have occurred where LPS on the cell surface of Gram-negative bacteria were stretched upon the ensuing repulsive force during interactions between bacteria and GO in the reaction medium. The bridging effects of LPS may have been responsible for the indentations that are observed on the surface of Gram-negative bacteria in the FESEM images in Fig. 4. Correspondingly, an investigation that was conducted to study the puncturing effects of AFM tip on the Gram-negative *Salmonella* Typhimurium managed to survive after multiple puncturing of their cell wall. Lipid bilayers and peptidoglycan layer of the bacteria are suggested to be self-repairing as it retains the integrity, viability and reproductive ability even after repeated puncturing of cell membrane [64].

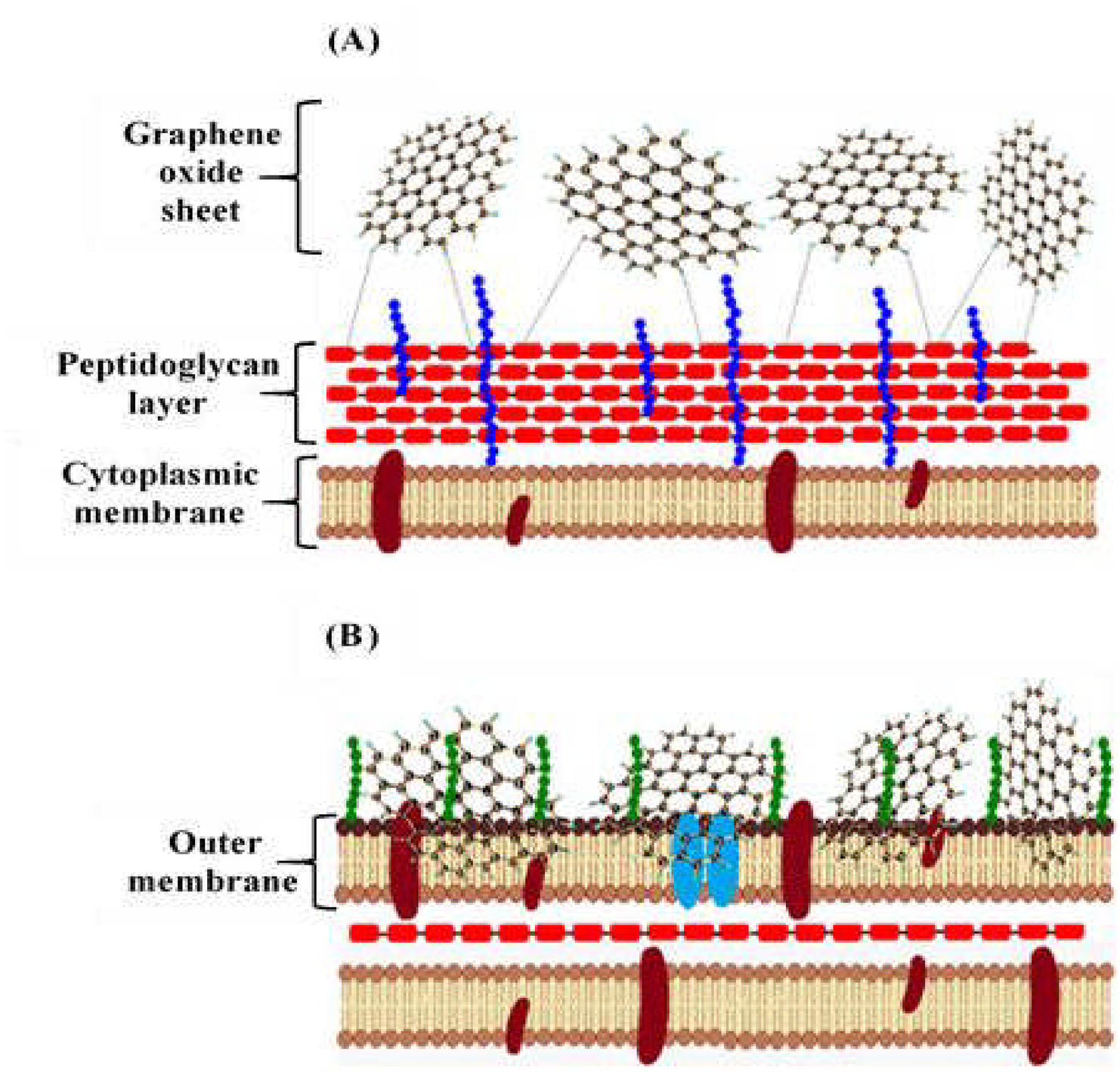

Fig. 7. Schematic diagram of the possible mechanism of action of GO towards Gram-positive and Gram-negative bacteria. (A) mechanical wrapping in Gram-positive bacteria and (B) membrane damage in Gram-negative bacteria.

4. Conclusion

The antibacterial activity of GO towards *S. aureus*, *E. faecalis*, *E. coli* and *P. aeruginosa* indicated that antibacterial activity of GO was concentration and time-dependent. Surface morphology of bacterial cells after exposure of GO showed evidence of membrane disruptions and bacterial entrapment under GO sheets that have contributed to cell death. Additional characterization with ATR-FTIR analysis proved that the interaction of GO with bacterial membrane occurs upon contact, resulting in changes in the IR spectra of untreated and treated bacterial culture. The antibacterial mechanism of GO towards bacteria differed between Gram-positive and Gram-negative bacteria, where the majority of bacterial inactivation of Gram-positive bacteria occurs through bacterial wrapping mechanism. On the other hand, inactivation of Gram-negative bacteria mainly occurs through physical contact which leads to membrane damage. The outer membrane layer in Gram-negative bacteria acted as a protective barrier against GO compared to Gram-positive bacteria. As the antibacterial effects of GO have enormous potential for antimicrobial applications, the mechanism of action of GO towards bacteria must be clearly elucidated to ensure complete bacterial inactivation.

Acknowledgements

This work was supported by BKP (BK095-2016) and UMRG (RP045-17AET) grants from University of Malaya and by Fundamental Research Grant Scheme (FP054-2016) from Ministry of Higher Education, Malaysia.

Compliance with Ethical Standards:

Funding: This study was funded by University of Malaya through BKP (BK095-2016) and UMRG (RP045-17AET) grants and by the Fundamental Research Grant Scheme (FP054-2016) from Ministry of Higher Education, Malaysia.

Conflict of Interest: Thiruchelvi Pulingam, Kwai Lin Thong, Md. Eaqub Ali, Jimmy Nelson Appaturi, Ignatius Julian Dinshaw, Zhan Yuin Ong and Bey Fen Leo declare that they have no conflict of interest.

Ethical approval: This article does not contain any studies with human participants or animals performed by any of the authors.

Informed consent: Informed consent was not obtained as no human participants were involved in this study.

References

1. Wu, X., et al., *Graphene oxide as an efficient antimicrobial nanomaterial for eradicating multi-drug resistant bacteria in vitro and in vivo.* Colloids and Surfaces B: Biointerfaces, 2017. **157**: p. 1-9.
2. Papi, M., et al., *Biomimetic antimicrobial cloak by graphene-oxide agar hydrogel.* Scientific reports, 2016. **6**(1): p. 12.
3. Zhou, S. and A. Bongiorno, *Origin of the chemical and kinetic stability of graphene oxide.* Scientific reports, 2013. **3**: p. 2484.
4. Liu, S., et al., *Stable aqueous dispersion of graphene nanosheets: noncovalent functionalization by a polymeric reducing agent and their subsequent decoration with Ag nanoparticles for enzymeless hydrogen peroxide detection.* Macromolecules, 2010. **43**(23): p. 10078-10083.
5. Liu, Z., et al., *PEGylated nanographene oxide for delivery of water-insoluble cancer drugs.* Journal of the American Chemical Society, 2008. **130**(33): p. 10876-10877.
6. Sun, X., et al., *Nano-graphene oxide for cellular imaging and drug delivery.* Nano research, 2008. **1**(3): p. 203-212.
7. Yang, K., et al., *Nano-graphene in biomedicine: theranostic applications.* Chemical Society Reviews, 2013. **42**(2): p. 530-547.
8. Allahverdiyev, A.M., et al., *Coping with antibiotic resistance: combining nanoparticles with antibiotics and other antimicrobial agents.* Expert review of anti-infective therapy, 2011. **9**(11): p. 1035-1052.
9. Vimbela, G.V., et al., *Antibacterial properties and toxicity from metallic nanomaterials.* International Journal of Nanomedicine, 2017. **12**: p. 3941.
10. Gao, Y., et al., *Impact of graphene oxide on the antibacterial activity of antibiotics against bacteria.* Environmental Science: Nano, 2017. **4**(5): p. 1016-1024.
11. Wang, Z., et al., *Carbon nanomaterials-based electrochemical aptasensors.* Biosensors and Bioelectronics, 2016. **79**: p. 136-149.
12. Pelin, M., et al., *Graphene and graphene oxide induce ROS production in human HaCaT skin keratinocytes: The role of xanthine oxidase and NADH dehydrogenase.* Nanoscale, 2018. **10**(25): p. 11820-11830.
13. Jalali, M., J. Zaborowska, and M. Jalali, *The Polymerase Chain Reaction: PCR, qPCR, and RT-PCR*, in *Basic Science Methods for Clinical Researchers*. 2017, Elsevier. p. 1-18.
14. Akhavan, O. and E. Ghaderi, *Toxicity of graphene and graphene oxide nanowalls against bacteria.* ACS Nano, 2010. **4**(10): p. 5731-6.
15. Deokar, A.R., et al., *Single-walled carbon nanotube coated antibacterial paper: preparation and mechanistic study.* Journal of Materials Chemistry B, 2013. **1**(20): p. 2639-2646.
16. Wang, L., C. Hu, and L. Shao, *The antimicrobial activity of nanoparticles: present situation and prospects for the future.* International journal of nanomedicine, 2017. **12**: p. 1227.
17. Hui, L., et al., *Availability of the basal planes of graphene oxide determines whether it is antibacterial.* ACS Appl Mater Interfaces, 2014. **6**(15): p. 13183-90.
18. Nanda, S.S., D.K. Yi, and K. Kim, *Study of antibacterial mechanism of graphene oxide using Raman spectroscopy.* Sci Rep, 2016. **6**: p. 28443.

19. Zou, F., et al., *Wrinkled Surface-Mediated Antibacterial Activity of Graphene Oxide Nanosheets.* ACS Appl Mater Interfaces, 2017.
20. Hou, W.-C., et al., *Antibacterial Property of Graphene Oxide: the Role of Phototransformation.* Environmental Science: Nano, 2017.
21. Huang, N., et al., *Simple room-temperature preparation of high-yield large-area graphene oxide.* International journal of nanomedicine, 2011. **6**: p. 3443.
22. Hummers Jr, W.S. and R.E. Offeman, *Preparation of graphitic oxide.* Journal of the American Chemical Society, 1958. **80**(6): p. 1339-1339.
23. Gurunathan, S., et al., *Antibacterial activity of dithiothreitol reduced graphene oxide.* Journal of Industrial and Engineering Chemistry, 2013. **19**(4): p. 1280-1288.
24. Guo, Z., et al., *Toxicity and transformation of graphene oxide and reduced graphene oxide in bacteria biofilm.* Science of The Total Environment, 2017. **580**: p. 1300-1308.
25. Gupta, V., et al., *Higher oxidation level in graphene oxide.* Optik - International Journal for Light and Electron Optics, 2017. **143**(Supplement C): p. 115-124.
26. Luo, Z., et al., *High Yield Preparation of Macroscopic Graphene Oxide Membranes.* Journal of the American Chemical Society, 2009. **131**(3): p. 898-899.
27. Shi, P., et al., *Supported cobalt oxide on graphene oxide: Highly efficient catalysts for the removal of Orange II from water.* Journal of Hazardous Materials, 2012. **229-230**(Supplement C): p. 331-339.
28. Zhang, M., et al., *Preparation of cobalt silicide on graphene as Pt electrocatalyst supports for highly efficient and stable methanol oxidation in acidic media.* Electrochimica Acta, 2015. **161**(Supplement C): p. 48-54.
29. Zhou, K., et al., *The influence of cobalt oxide–graphene hybrids on thermal degradation, fire hazards and mechanical properties of thermoplastic polyurethane composites.* Composites Part A: Applied Science and Manufacturing, 2016. **88**(Supplement C): p. 10-18.
30. Chaiyakun, S., et al., *Preparation and characterization of graphene oxide nanosheets.* Procedia Engineering, 2012. **32**: p. 759-764.
31. Perreault, F., et al., *Antimicrobial Properties of Graphene Oxide Nanosheets: Why Size Matters.* ACS Nano, 2015. **9**(7): p. 7226-36.
32. Nyquist, R.A. and R.O. Kagel, *Handbook of infrared and raman spectra of inorganic compounds and organic salts: infrared spectra of inorganic compounds*. Vol. 4. 2012: Academic press.
33. Valentini, L., et al., *Deposition of amino-functionalized polyhedral oligomeric silsesquioxanes on graphene oxide sheets immobilized onto an amino-silane modified silicon surface.* Journal of Materials Chemistry, 2012. **22**(13): p. 6213-6217.
34. Thirunavukkarasu, R., et al., *Isolation of bioactive compound from marine seaweeds against fish pathogenic bacteria Vibrio alginolyticus (VA09) and characterisation by FTIR.* Journal of Coastal Life Medicine, 2013. **1**(1): p. 26-33.
35. Venkatasubbu, G.D., et al., *Toxicity mechanism of titanium dioxide and zinc oxide nanoparticles against food pathogens.* Colloids and Surfaces B: Biointerfaces, 2016. **148**: p. 600-606.
36. Krishnamoorthy, K., et al., *Antibacterial efficiency of graphene nanosheets against pathogenic bacteria via lipid peroxidation.* The Journal of Physical Chemistry C, 2012. **116**(32): p. 17280-17287.
37. Liu, S., et al., *Antibacterial activity of graphite, graphite oxide, graphene oxide, and reduced graphene oxide: membrane and oxidative stress.* ACS Nano, 2011. **5**(9): p. 6971-80.

38. Zhao, J., et al., *Graphene in the aquatic environment: adsorption, dispersion, toxicity and transformation.* Environmental science & technology, 2014. **48**(17): p. 9995-10009.
39. Tu, Y., et al., *Destructive extraction of phospholipids from Escherichia coli membranes by graphene nanosheets.* Nat Nanotechnol, 2013. **8**(8): p. 594-601.
40. Hu, W., et al., *Graphene-based antibacterial paper.* ACS nano, 2010. **4**(7): p. 4317-4323.
41. Li, R., et al., *Identification and Optimization of Carbon Radicals on Hydrated Graphene Oxide for Ubiquitous Antibacterial Coatings.* ACS Nano, 2016. **10**(12): p. 10966-10980.
42. Barenfanger, J. and C.A. Drake, *Interpretation of Gram stains for the nonmicrobiologist.* Laboratory medicine, 2001. **32**(7): p. 368-375.
43. Davis, R. and L. Mauer, *Fourier transform infrared (FT-IR) spectroscopy: a rapid tool for detection and analysis of foodborne pathogenic bacteria.* Current research, technology and education topics in applied microbiology and microbial biotechnology, 2010. **2**: p. 1582-1594.
44. Rebuffo, C.A., et al., *Reliable and rapid identification of Listeria monocytogenes and Listeria species by artificial neural network-based Fourier transform infrared spectroscopy.* Applied and environmental microbiology, 2006. **72**(2): p. 994-1000.
45. Kuhm, A.E., et al., *Application of Fourier transform infrared spectroscopy (FT-IR) for the identification of Yersinia enterocolitica on species and subspecies level.* Applied and Environmental Microbiology, 2009.
46. Kannan, S., *FT-IR and EDS analysis of the seaweeds Sargassum wightii (brown algae) and Gracilaria corticata (red algae).* International Journal of Current Microbiology and Applied Sciences, 2014. **3**(4): p. 341-351.
47. Bhat, R., *Potential use of fourier transform infrared spectroscopy for identification of molds capable of producing mycotoxins.* International journal of food properties, 2013. **16**(8): p. 1819-1829.
48. Garip, S., F. Bozoglu, and F. Severcan, *Differentiation of mesophilic and thermophilic bacteria with Fourier transform infrared spectroscopy.* Applied spectroscopy, 2007. **61**(2): p. 186-192.
49. Suzuki, H., et al., *Functional roles of D2-Lys317 and the interacting chloride ion in the water oxidation reaction of photosystem II as revealed by Fourier transform infrared analysis.* Biochemistry, 2013. **52**(28): p. 4748-4757.
50. Lebedeva, O., et al., *Hybrid ion-exchange membranes based on heteroaromatic sulfonic acid derivatives.* Petroleum chemistry, 2015. **55**(5): p. 333-338.
51. Wong, P., et al., *Infrared spectroscopy of exfoliated human cervical cells: evidence of extensive structural changes during carcinogenesis.* Proceedings of the National Academy of Sciences, 1991. **88**(24): p. 10988-10992.
52. Brown, L., et al., *Through the wall: extracellular vesicles in Gram-positive bacteria, mycobacteria and fungi.* Nature Reviews Microbiology, 2015. **13**(10): p. 620.
53. Liang, H., et al., *Metabolic labelling of the carbohydrate core in bacterial peptidoglycan and its applications.* Nature communications, 2017. **8**: p. 15015.
54. Kell, A.J., et al., *Vancomycin-modified nanoparticles for efficient targeting and preconcentration of Gram-positive and Gram-negative bacteria.* Acs Nano, 2008. **2**(9): p. 1777-1788.
55. Silhavy, T.J., D. Kahne, and S. Walker, *The bacterial cell envelope.* Cold Spring Harbor perspectives in biology, 2010. **2**(5): p. a000414.
56. Kommineni, S., et al., *Bacteriocin production augments niche competition by enterococci in the mammalian gastrointestinal tract.* Nature, 2015. **526**(7575): p. 719.

57. Chiller, K., B.A. Selkin, and G.J. Murakawa. *Skin microflora and bacterial infections of the skin*. in *Journal of Investigative Dermatology Symposium Proceedings*. 2001. Elsevier.
58. Delcour, A.H., *Outer membrane permeability and antibiotic resistance.* Biochimica et Biophysica Acta (BBA)-Proteins and Proteomics, 2009. **1794**(5): p. 808-816.
59. Kamio, Y. and H. Nikaido, *Outer membrane of Salmonella typhimurium: accessibility of phospholipid head groups to phospholipase c and cyanogen bromide activated dextran in the external medium.* Biochemistry, 1976. **15**(12): p. 2561-2570.
60. Nikaido, H., *Molecular basis of bacterial outer membrane permeability revisited.* Microbiology and molecular biology reviews, 2003. **67**(4): p. 593-656.
61. Romero-Vargas Castrillón, S., et al., *Interaction of graphene oxide with bacterial cell membranes: insights from force spectroscopy.* Environmental Science & Technology Letters, 2015. **2**(4): p. 112-117.
62. Dreyer, D.R., A.D. Todd, and C.W. Bielawski, *Harnessing the chemistry of graphene oxide*. Chemical Society Reviews, 2014. **43**(15): p. 5288-5301.
63. Camesano, T.A. and B.E. Logan, *Probing bacterial electrosteric interactions using atomic force microscopy.* Environmental Science & Technology, 2000. **34**(16): p. 3354-3362.
64. Suo, Z., et al., *Bacteria survive multiple puncturings of their cell walls.* Langmuir, 2009. **25**(8): p. 4588-4594.